journal of the mechanical behavior of biomedical materials 106 (2020) 103744

Contents lists available at ScienceDirect

Journal of the Mechanical Behavior of Biomedical Materials

journal homepage: http://www.elsevier.com/locate/jmbbm

# Ultra-high-purity iron is a novel and very compatible biomaterial

Luqman Khan [a], Katsumi Sato [b], Shinichi Okuyama [c], Takeshi Kobayashi [d], Kazumasa Ohashi [a], Katsuya Hirasaka [e], Takeshi Nikawa [f], Kunio Takada [g], Atsushi Higashitani [a,*], Kenji Abiko [g]

[a] Graduate School of Life Sciences, Tohoku University, Sendai, 980-8577, Japan
[b] Tohoku Rosai Hospital, Sendai, 981-8563, Japan
[c] Home Doctors Okuyama, Sendai, 981-3122, Japan
[d] Graduate School of Medicine, Nagoya University, Nagoya, 466-8550, Japan
[e] Graduate School of Fisheries and Environmental Sciences, Nagasaki University, Nagasaki, 852-8521, Japan
[f] Institute of Medical Nutrition, Tokushima University Medical School, Tokushima, 770-8503, Japan
[g] Institute for Materials Research, Tohoku University, Sendai, 980-8577, Japan

ARTICLE INFO

*Keywords:*
Cell differentiation
Cell proliferation
Fe
Mesenchymal stem cells
Myoblast

ABSTRACT

Metals and alloys are used widely in bone prosthetic materials, stents and dental tissue reconstructions. The most common materials are stainless steels and cobalt-chromium-nickel and titanium alloys. These alloys can be easily deformed but are hard to break. However, their affinity for cells and tissues is very low. In addition, they can sometimes provoke unexpected metal allergies. Iron is an abundant trace element essential for humans. However, excess amounts in particular of $Fe^{2+}$ ions are toxic. We previously succeeded in obtaining 99.9996% ultra-high-purity iron (ABIKO iron). The chemical properties of ABIKO iron are completely different from that of conventional pure iron. For example, the reaction rate in hydrochloric acid is very slow and there is barely any corrosion. Here, we found that, in the absence of any type of coating, mammalian cells could easily attach to, and normally proliferate and differentiate on, ABIKO iron. On the other hand, cell densities and proliferation rate of the surfaces of plates made from Co–Cr–Mo or Ti–6Al–4V were significantly reduced. In addition, several stress and iron response genes, HSP70, SOD1, ATM and IRP2 did not change in the cells on ABIKO iron, while these genes were induced with exogenous application of $FeSO_4$. Cells also secreted and fastened some organics on ABIKO iron. In vitro collagen binding assay showed that ABIKO iron binds higher amount of collagens. These findings highlight ABIKO iron as a novel biocompatible prosthetic material.

## 1. Introduction

With advances in medical technology, new therapeutic materials are being developed and improved to be human friendly. In particular, the use of metallic materials in implants, stents and implantable devices is increasing because of their excellent processability and strength (Niinomi, 2002; Sidambe, 2014; Vasconcelos et al., 2016). However, metallic materials have problems such as corrosion and toxicity when used for a long time in the human body (Hanawa, 2004; Lai et al., 2008; Chou et al., 2013; Gomes et al., 2011; Costa et al., 2019). Therefore, various corrosion-resistant alloys such as stainless steels (Fe–Cr-(Ni) alloys), Co–Cr–Mo alloys and Ti–6Al–4V alloys have been developed, but problems such as metallic allergies remain (Fage et al., 2016; Pacheco, 2019; Tibau et al., 2019). Furthermore, the surfaces of metallic materials and alloys are poorly compatible with cells and tissues (Bacakova et al., 2011). Surface-treatment materials such as hydroxyapatite, calcium carbonate and multi-elements are currently being devised, but there is still concern about the stability of these coating materials (Besinis et al., 2017; Bang et al., 2019; Santos-Coquillat et al., 2019).

Iron (Fe) is the most abundant transition metal in the human body, which contains 4–5 g (Oliveira et al., 2014). Like haemoglobin, it is essential for the catalytic centres of several enzymes involved in electron transfer and DNA metabolism. However, excess $Fe^{2+}$ ions react with hydrogen peroxide to produce reactive oxygen species. Conventional pure iron is more easily corroded and produces $Fe^{2+}$ ions than stainless steels and alloys. This leads to cytotoxicity and causes an inflammatory response and cell death in vivo (Puntarulo, 2005). The presence of impurities is one of the causes of metal corrosion. In response to this problem, we have succeeded in obtaining 99.9996% ultra-high-purity

* Corresponding author.
*E-mail address:* atsushi.higashitani.e7@tohoku.ac.jp (A. Higashitani).

https://doi.org/10.1016/j.jmbbm.2020.103744
Received 27 October 2019; Received in revised form 10 February 2020; Accepted 18 March 2020
Available online 27 March 2020

ABIKO iron in a newly designed induction-melting furnace by using ultra-high vacuum technology (Abiko et al., 1998; Abiko et al., 2002; BAM (Germany)). Surprisingly, the chemical properties of ABIKO iron and conventional pure iron are completely different. Not only is the surface of ABIKO iron very smooth and shiny, but also this iron barely reacts in hydrochloric acid or in copper sulphate solution, compared with those of conventional iron. In addition, ABIKO iron is flexible, easy to deform and hard to break, because it contains few impurities (Abiko et al., 1998, 2002). Here, we address the biocompatibility of ABIKO iron in mammalian cell culture in vitro. In this study, mammalian cell attachment, proliferation, and differentiation were successful with ABIKO iron without any type of surface treatment, but not with Co–Cr–Mo and Ti–6Al–4V alloys.

## 2. Experimental

### 2.1. Materials

Ultra-high-purity ABIKO iron, as described earlier (Abiko et al., 1998, 2002), and Ti–6Al–4V extra-low interstitial ELI (ASTM F136) and Co–Cr–Mo (ASTM F1537) were used. These metals were rinsed carefully in 100% acetone and then washed in 70% ethanol. After being washed, the metals were air dried on a clean bench and placed into the cell-culture dishes (Greiner Bio-One 627 160 and 628 160, Tokyo/Japan).

### 2.2. Cell culture

Madin-Darby canine kidney (MDCK) cells that stably express YFP (yellow fluorescent protein)-human keratin-8 (MDCK–YFP-keratin-8) cells (Fujiwara et al., 2016) were cultured by using standard methods in Dulbecco's Modified Eagle's Medium (DMEM) – high glucose (Sigma-Aldrich, St. Louis/U.S.A. D5796), supplemented with 10% foetal bovine serum (FBS) (Thermo Fisher Scientific, MA/U.S.A.) and 1% penicillin and streptomycin (P–S) (Nacalai Tesque Inc., Kyoto/Japan). The MDCK cell culture was incubated at 37 °C in a 5% $CO_2$ humidified atmosphere. The cells were transferred to fresh medium after reaching 70%–80% confluence. The cells were observed under fluorescence microscope (BX51 Olympus, Tokyo/Japan) equipped with a CCD camera (DP73 Olympus, Tokyo/Japan). The relative confluence of cells was based on the YFP fluorescence. The cellular boundaries were the measure of the confluency by Image J Fiji software.

Murine myoblast C2C12 cells were cultured in DMEM containing 10% FBS and 1% P–S at 37 °C with 5% CO2. At a confluence of 80%–100%, C2C12 myoblastic cells were fused by shifting medium to DMEM containing 2% donor horse serum (MP Biomedicals, CA/U.S.A.). Cells were maintained in 2% horse serum (differentiation medium) for additional 5 days at 37 °C in a 5% $CO_2$ humidified atmosphere (Yoshimura et al., 2018). To stain the C2C12 cell line we used calcein AM solution (Dojindo Molecular Technologies, Inc., Kumamoto/Japan). Calcein AM solution is used to label live cells, which can then be detected and further analysed by using green fluorescence imaging. To analyse myotubes differentiation, expression levels of skeletal myosin were monitored by immunoblotting using the anti-fast-twitch type myosin heavy chain antibodies (Sigma Aldrich, St. Louis, MO, USA), the anti-GAPDH as control (Santa Cruz Biotechnology, Santa Cruz, CA, USA), and the secondary antibodies sheep anti-mouse IgG and donkey anti-rabbit IgG (GE Healthcare, Little Chalfont, UK), respectively (Yoshimura et al., 2018).

Murine bone marrow-derived Mesenchymal stem cells (MSCs) were obtained from Gibco/Thermo Fisher Scientific (MA, USA) and cultured in MSC growth medium composed of Dulbecco's modified Eagle's medium: Nutrient Mixture F-12 (DMEM/F-12, Thermo Fisher Scientific, MA, USA) supplemented with 10% FBS, GlutaMAX-1 (Thermo Fisher Scientific, MA, USA) and gentamycin (5 μg/ml, Thermo Fisher Scientific, MA, USA). After the cell confluency had reached 50%, the medium was switched to osteogenic differentiation medium (MSC growth medium supplemented with 10 mM β-glycerophosphate (FUJIFILM Wako Pure Chem. Co., Osaka, Japan), 50 μM ascorbic acid (FUJIFILM Wako Pure Chem. Co., Osaka, Japan), and 10 nM dexamethasone (FUJIFILM Wako Pure Chem. Co., Osaka, Japan).

To examine if ABIKO-iron affect the osteoblastic differentiation of murine MSCs, we analysed the expression of specific markers during osteogenic differentiation of MSCs cultured on ABIKO-iron while comparing with those on a plastic tissue culture dish (C.D.). MSCs were seeded on ABIKO-iron or C.D. in the MSC growth medium at a density of $2 \times 10^4$ cells/cm$^2$ and next day the medium was replaced with the osteogenic differentiation medium. After 6-day culture in the osteogenic differentiation medium, cells were scraped, and total RNA was isolated using NucleoSpin RNA kit (TaKaRa Bio). Real-time quantitative RT-PCR was performed as described below. We also used alizarin red S solution (Sigma-Aldrich, St. Louis/U.S.A.), an anthraquinone dye, which has been used widely to evaluate calcium deposition in cell culture. Briefly, the cells were plated for 21 days at 37 °C in a 5% $CO_2$ humidified atmosphere and treated as described above to promote osteogenic differentiation. The medium was removed and the cells were washed gently with 1 × Dulbecco's PBS three times. The MSCs were then fixed in 4% formaldehyde for 15 min at room temperature. The fixative was removed and the cells were washed three times with distilled water. The cells were removed from the metal surface or the culture dish surface, and then stained for 30 min with 1 mL of 40 mM alizarin red S in a new culture dish at room temperature. The dye was removed and the cells were washed five times with distilled water.

### 2.3. SEM and EDS

Culture cells on the metal surface were fixed with 2% glutaraldehyde in 30 mM HEPES–KOH (pH 7.5) for 60 min. After dehydration with an ethanol series, the samples were dried in a $CO_2$ critical point dryer. The surface of the samples was coated with an osmium surface coating (Meiwafosis Co. Ltd., Tokyo/Japan) for EDS quantification of light elements. The samples were analysed by field emission SEM with EDS (JSM-7800F, JEOL Ltd. Tokyo/Japan).

### 2.4. Gene expression analysis

To examine the effects of ABIKO-iron plate and $FeSO_4$ application on expression of several stress response genes, MDCK-YFP-keratin 8 cells were cultured on ABIKO iron and S45C steel, and in the presence of 0.01 mM–5 mM $FeSO_4$, respectively. The cells were cultured for 24 h after $FeSO_4$ application, after which total RNA was extracted with Trizol reagent (Invitrogen). Real-time quantitative RT-PCR was performed with a PrimeScript II 1st strand cDNA Synthesis Kit (TaKaRa Bio) and SYBR Premix Ex Taq II (TaKaRa Bio), in a CFX96 Real-Time System (Bio-Rad Laboratories), with the following forward and reverse primers: 5′-TGC TGA GGA TCA TCA ACG AG -3′ and 5′-GCT TGA ACT CCT CCA CGA AG-3′ for HSP70, 5′-AGT GGG CCT GTT GTG GTA TC-3′ and 5′-AGT CAC ATT GCC CAG GTC TC-3′ for SOD1, 5′-GAA GAA GGA ACG GTG CTC AG-3′ and 5′-GGT TAA AAA CGA AGG CCA CA-3′ for ATM, 5′-CCA GCG GAG TGT TAC CGT AT -3′ and 5′-AAT TGG CAC GAA CAC AAT CA -3′ for IRP2, 5′-TTC CGA GTG GCA GCT GAG ATG TTT -3′ and 5′-TGC TGG CAA AGT AGA AGA GGG CAA -3′ for BAX, 5′-TTC ATT ATT CAG GCC TGC CGA GG -3′ and 5′-TTC TGA CAG GCC ATG TCA TCC TCA -3′ for caspase-3, and 5′-ATC ACT GCC ACC CAG AAG AC -3′ and 5′-GGC AGG TCA GAT CCA CAA CT -3′ for GAPDH as internal control.

We also performed real-time quantitative RT-PCR to monitor the expression of specific markers during osteogenic differentiation of MSCs with the following primer set. 5′-CAC TGG CGG TGC AAC AAG A -3′ and 5′-ATG ACG GTA ACC ACA GTC CCA TC -3′ for Runx2, 5′-CGC ACG CGA TGC AAC ACC AC -3′ and 5′-TGC CCA CGG ACT TCC CAG CA -3′ for Alpl, 5′-CCG GGA GCA GTG TGA GCT TA -3′ and 5′-TAG ATG CGT TTG TAG GCG GTC -3′ for Bglap, 5′-CTC CAA TCG TCC CTA CAG TCG -3′ and 5′-

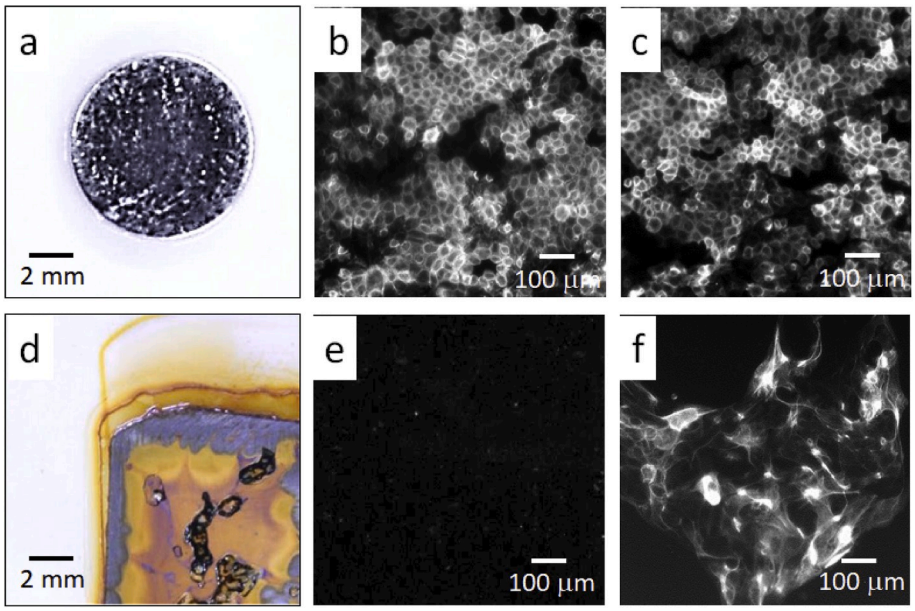


**Fig. 1.** MDCK–YFP-keratin-8 cells were cultured with ABIKO iron or a commercial carbon steel (S45C) plate for 3 days.

CCA AGC TAT CAC CTC GGC C -3′ for Spp1, and 5′-TGT GTC CGT CGT GGA TCT GA -3′ and 5′-TTG CTG TTG AAG TCG CAG GAG -3′ for GAPDH as internal control.

### 2.5. In vitro collagen binding assay

To analyse affinity of collagen on the metal surface, the metal plate was soaked in 3 ml freshly diluted FITC labelled collagen solution (at final concentration of 0.01 mg/ml) with PBS (Bovine Type I collagen, Collagen Research Center, Japan) for 1 h at room temperature. After rinsing the surface with distilled water, FITC intensity was monitored with a fluorescent stereo microscopy (Nikon, Tokyo/Japan). The intensity was calculated by Image J Fiji software.

### 2.6. Statistical analysis

All experiments were performed in at least triplicate for each biological sample and metal material. Sample sizes (n) are specified in the figure legends for all of the quantitative data. RStudio software (https://www.rstudio.com) was used to determine statistical significance. Statistical analysis was performed using a Student's two-tailed t-test and one-way ANOVA followed by Tukey post hoc test. The minimum p-value for significance was 0.05. Similar alphabet(s) in any two groups indicate no significance and different alphabets in any two groups represent significant difference between the two groups.

## 3. Results and discussion

### 3.1. MDCK cell proliferation on ultra-high-purity ABIKO iron and no toxicity of $Fe^{2+}$ ion released

Because conventional transmitted light cannot be used for live cell imaging on metal surfaces, we used reflection fluorescence imaging with MDCK–YFP-keratin-8 (Fujiwara et al., 2016). This YFP recombinant line is less morphologically affected and gives brighter signals, compared with other YFP fusion of cytoskeletal proteins (Fujiwara et al., 2016). Cells at $1 \times 10^5$ were freshly inoculated into 35-mm culture dishes, into each of which we placed a metal plate (approximately 0.5 $cm^2$ × 0.1 cm thickness), and then cultured for 3 days in DMEM growth media at 37 °C until the controls (cells in dishes without metal plates) were nearly confluent. Intriguingly, the cells proliferated and became confluent not only on each culture dish, as in the controls, but also on the ABIKO iron surface and culture dish surface (Fig. 1b and c). In contrast, the surface of a commercial carbon steel (S45C) plate was corroded and cells did not grow on the plate (Fig. 1d and e). In addition, cells on the culture dish with the S45C plate showed growth inhibition and abnormal shape

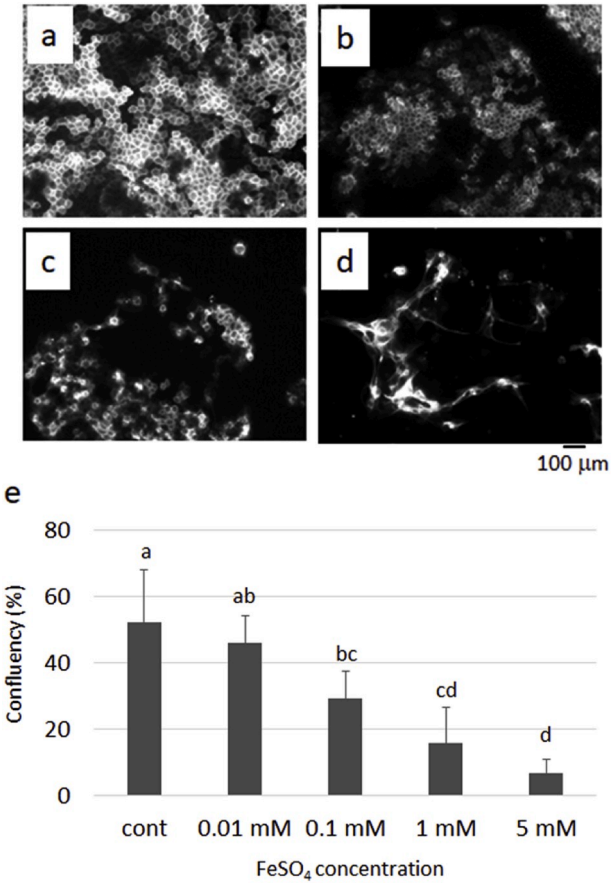


**Fig. 2.** $Fe^{2+}$ ions inhibited the growth and survival of MDCK–YFP-keratin-8 cells.

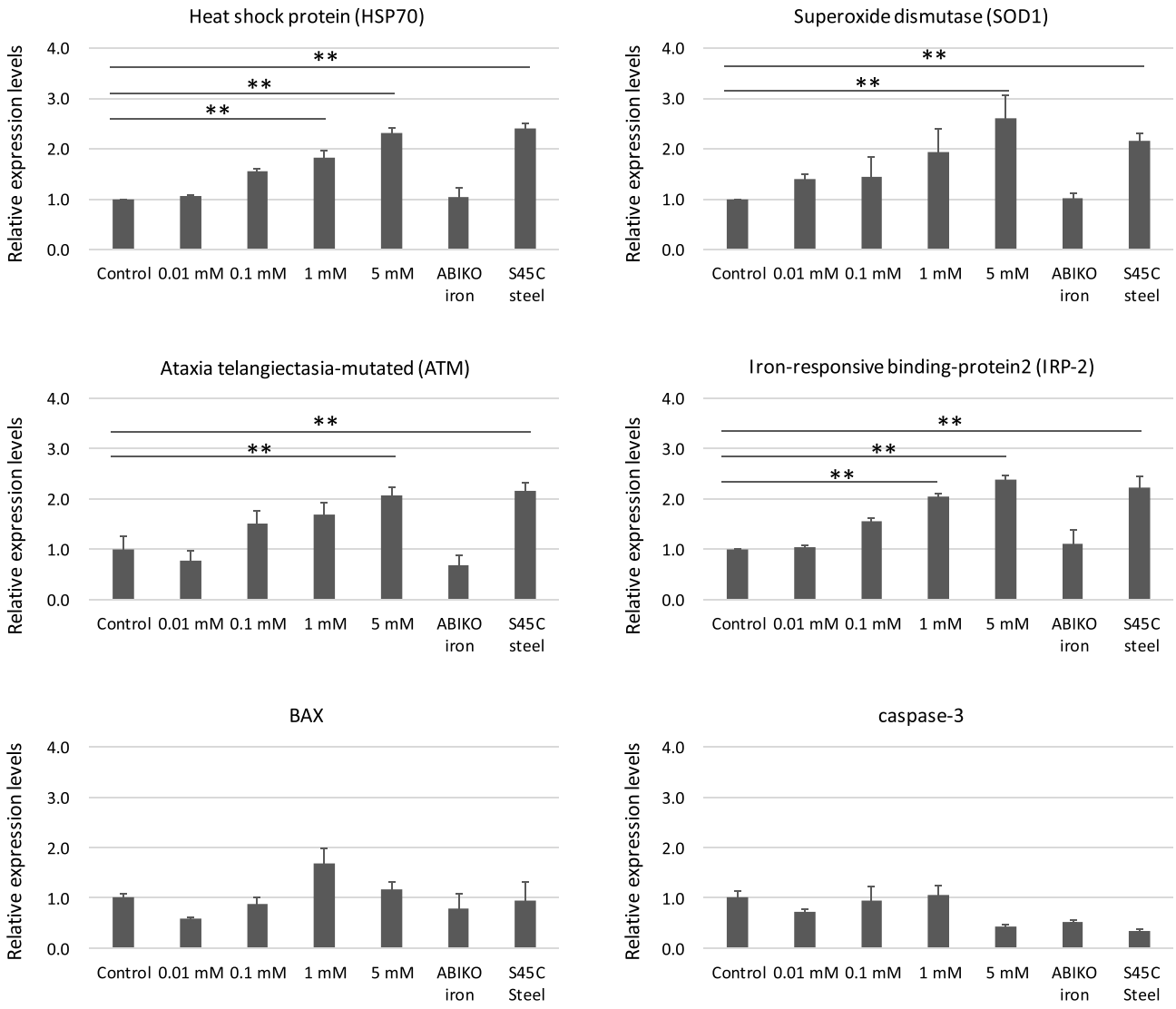


**Fig. 3.** Real-time qRT-PCR analysis of changes in gene expression induced by ABIKO iron, S45C steel, and $FeSO_4$ in MDCK cells.

(Fig. 1f). Induction of oxidative stress mediated by excess iron ions (Halliwell and Gutteridge, 1990) appears to lead cells to proliferation defects and death. Similarly, survival of MDCK–YFP-keratin-8 cells was significantly reduced by the application of exogenous $FeSO_4$ at a final concentration of 0.1 mM or more (Fig. 2). At the final concentration of 5.0 mM, the cell shape was abnormal as in the S45C plate, and the number of cells was reduced to approximately 10% from inoculum size (control $6.3 \times 10^5$ cells, 0.01 mM $5.5 \times 10^5$, 0.1 mM $3.5 \times 10^5$, 1.0 mM $1.9 \times 10^5$, and 5.0 mM $0.8 \times 10^3$).

We also measured the concentration of Fe ions eluted in the medium after 3 days of culture. The concentration was significantly increased in the supernatant from culture with S45C plate ($3.65 \pm 0.81$ mmol), but not in that form culture with an ABIKO iron plate ($0.029 \pm 0.026$ mmol) as compared with that from culture medium without metal plate ($0.013 \pm 0.009$ mmol).

Gene expression analysis showed that MDCK cells on ABIKO iron plate did not induce several stress response genes tested, such as heat shock protein HSP70, superoxide dismutase SOD1 and ataxia telangiectasia-mutated ATM genes (Fig. 3). Similarly, iron-responsive element-binding protein IRP2 did not change in MDCK cells on ABIKO iron. On the other hand, the expression levels of these genes significantly increased in the cells on the culture dish with S45C plate and exogenously applying of $FeSO_4$ solution, but BAX and caspase-3 activation was not observed with S45C and $FeSO_4$ treatment. Upregulation of BAX and caspase-3 genes has been reported in apoptotic cell death of the MDCK cells treated with a mycotoxin, ochratoxin A (Li et al., 2019). These results suggest that excess Fe ions ($\leq$5 mM) elicited a general stress response and cell death but did not, or only little, apoptosis. In contrast, ABIKO iron is sufficiently biocompatible, does not corrode, and does not carry the risk of toxicity from excess Fe ions produced in the culture medium.

### 3.2. *MDCK–YFP-keratin-8 cells cultured on general use alloy plates and ABIKO iron thin wires*

As compared with the MDCK cells on the surface of the ABIKO plate, the cell densities on the surfaces of plates made from Co–Cr–Mo or Ti–6Al–4V (materials that are in general medical use) were reduced significantly compared with those on the surface of the ABIKO plate (Fig. 4). In addition, under the culture conditions we used, the cell densities on the culture dishes in the presence of either of these alloys were reduced significantly compared with those on the control and ABIKO culture dishes. The fold change of cell number after 3 days of culture reached to $10.9 \pm 0.6$ control culture dish (C.D.), $10.7 \pm 0.3$ ABIKO-iron surface, $10.9 \pm 0.7$ C.D. with ABIKO iron, $0.35 \pm 0.16$ Cr–Co–Mo surface, $6.2 \pm 1.6$ C.D. with Cr–Co–Mo, $0.65 \pm 0.53$

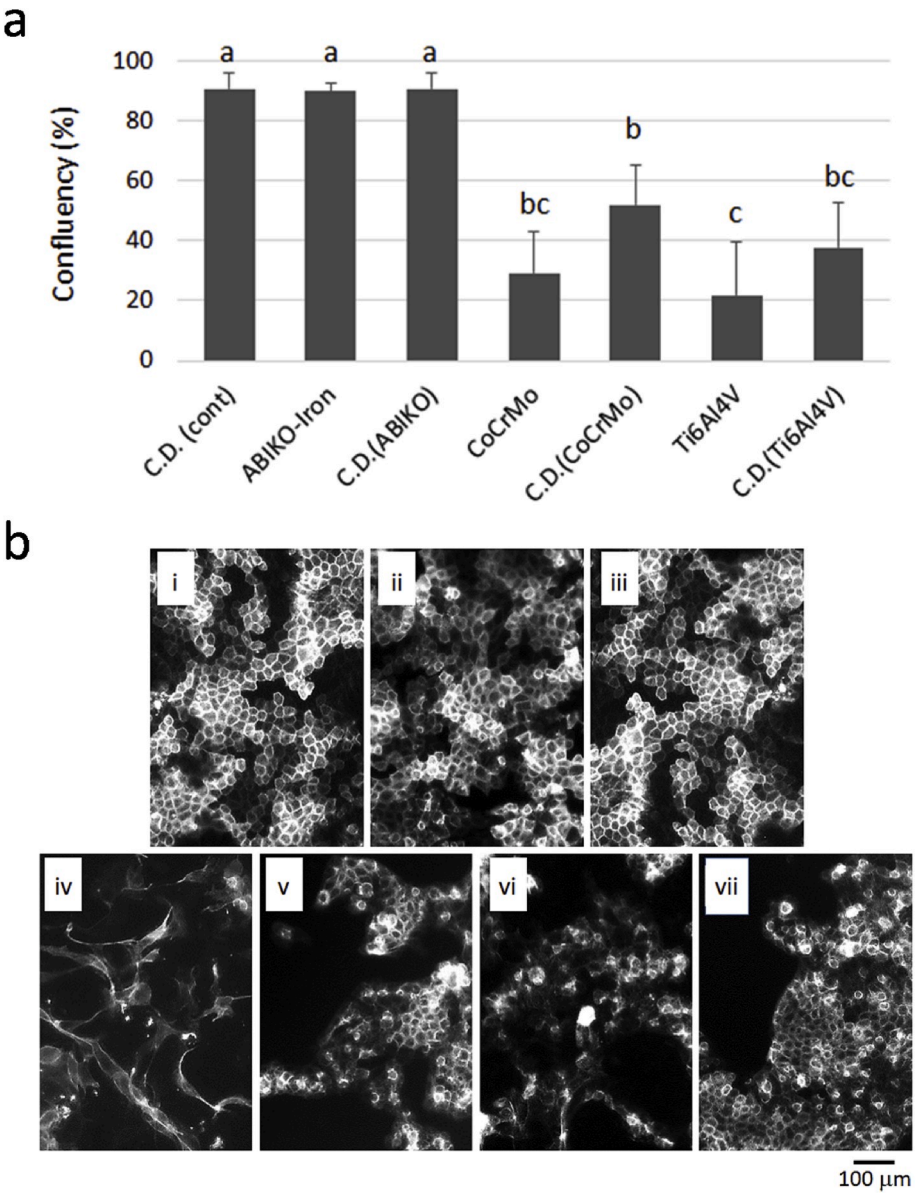


**Fig. 4.** Culture of MDCK–YFP-keratin-8 cells for 3 days after inoculation.

Ti–6Al–4V surface, and 4.5 ± 1.8 C.D. with Ti–6Al–4V. It was possible that toxic metal ions were released from these uncoated alloys into the in vitro culture medium (Marini et al., 2015; Wang et al., 2017). Furthermore, cell shape was normal on the ABIKO iron plates, but the cells were expanded abnormally on the Co–Cr–Mo plates and blurred in the images under fluorescent microscope, with small YFP-keratin-8-dotted signals, on the Ti–6Al–4V plate (Fig. 4). These results show that cells did not grow well on the surface of both alloys.

In order to evaluate whether the ABIKO iron can maintain high cell affinity in various shapes such as metal stents, a thin coiled wire made of ABIKO iron was placed in a culture dish and MDCK cells were newly inoculated. After 3 days of culture, the cells were mainly observed on the wire touching the bottom of the plate (Fig. 5b). The wire was then transferred to a new DMEM culture dish without additional cell inoculation. After 5 days of incubation, the cell grew well, moved, and spread throughout the wire (Fig. 5c and d). These results suggest that high cytophilicity of ABIKO iron could be maintained not only on plates, but also in stent shapes made of many thin wires.

### 3.3. Cell morphology on metal plates with scanning electron microscopy

The MDCK–YFP-keratin-8 cells were observed by scanning electron microscopy (SEM) to elucidate the cell attachment and structure on each metal plate. Normal, confluent MDCK cells were firmly attached to the ABIKO iron plates (Fig. 6a). When cells were diluted four-fold, inoculated into the dishes and cultured for 3 days at 37 °C, an abundance of normal, isotropically proliferating cells was observed on the ABIKO iron plates (Fig. 6b and c). In addition, thin films were frequently observed on the ABIKO iron (red dotted area in Fig. 6c). This suggested that the extracellular matrix released by the cells was well adsorbed to the ABIKO iron as a scaffold. In contrast, irregular, anisotropically spread cells were observed on both the Co–Cr–Mo plates and the Ti–6Al–4V plates, and the lamellipodia were widely expanded on cells on the Co–Cr–Mo plates (Fig. 6d and e). There were few, or no, cells in the growth phase on either of these types of alloy plates (Fig. 6d, f). Furthermore, on the Ti–6Al–4V plate, cell adhesion was very poor, and many of the cell bodies had been retracted, releasing numerous blebs (Fig. 6f), suggesting the progression of apoptotic cell death on the plates (Wickman et al., 2013). In addition, because only partial adhesion was

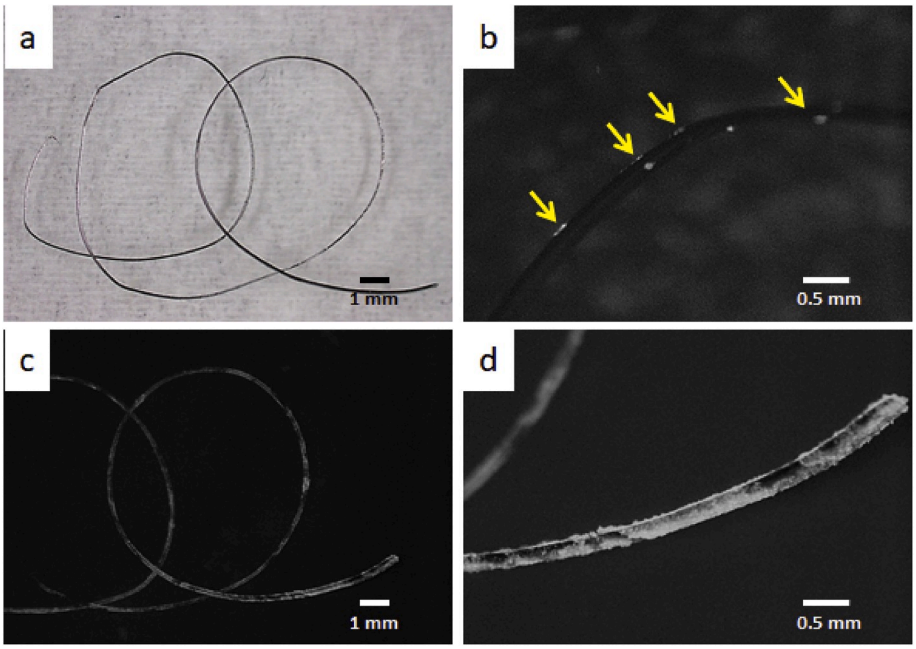


**Fig. 5.** Culture of MDCK–YFP-keratin-8 cells on thin coiled wire made of ABIKO iron.

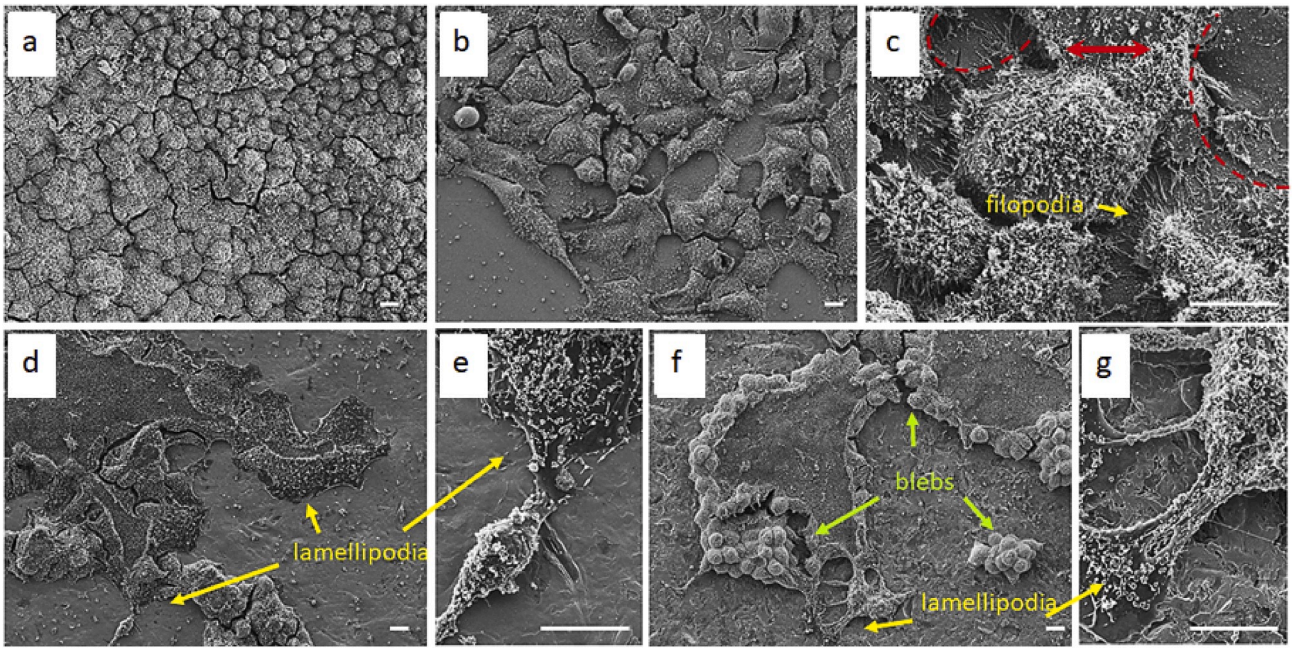


**Fig. 6.** Scanning electron microscope images of MDCK–YFP-keratin-8 cells cultured for 3 days after inoculation.

possible, stretched lamellipodia were observed (Fig. 6g).

We also noticed differences in the roughness of each metal surface. The surface of ABIKO iron was the smoothest (Supplementary Fig. 1); this may have been one of the factors increasing cell adhesion and proliferation. We also performed energy-dispersive X-ray spectroscopy (EDS) analyses on each metal surface (Supplementary Figs. 2–4). The atoms % of carbon, nitrogen, and oxygen were clearly increased in the region where cells were present on all metal surfaces. Even in the thin-film substance between cells on the surface of ABIKO iron, fewer but significant atoms % of carbon, nitrogen and oxygen atoms were detected compared to the backside area of ABIKO iron without cell growth (Supplementary Fig. 2, ROI002 and ROI1b). These results indicated that MDCK cells adhered directly to the ABIKO iron surface and grew well while secreting and fastening some organics such as collagens (as represented by the thin-film-like substances); this phenomenon was not observed in the case of the other alloys (Supplementary Figs. 3 and 4). In vitro collagen binding analysis also showed that ABIKO iron can bind much more FITC-labelled collagens than slide glass and Ti–6Al–4V plate (Fig. 7).

### 3.4. Mammalian cell differentiation on ABIKO iron plate

To assess the biocompatibility of ABIKO iron for cell differentiation, we monitored myogenic differentiation (of C2C12 myoblastoma cells) and osteogenic differentiation (of murine mesenchymal stem cells, MSCs). Similarly, to MDCK cells, C2C12 myoblasts proliferated well and

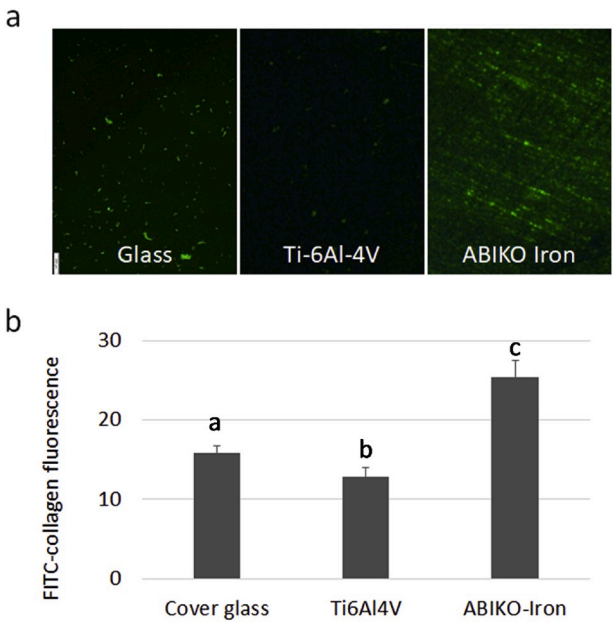


**Fig. 7.** In vitro collagen binding on ABIKO iron plate.

were confluent by 3 days on the ABIKO plates (Fig. 8). Furthermore, when differentiation medium was applied to confluent C2C12 cells, differentiated myotubes expressed muscle myosin appeared on the ABIKO iron plates after 5 more days of culture. The expression levels of fast-twitch type myosin heavy chain were slightly lower in the cells on the ABIKO iron plates compared with those of control plastic dishes (Fig. 8).

Likewise, MSCs differentiated into osteogenic cells on the ABIKO iron plates and on the surfaces of the culture dishes in the presence of ABIKO iron 21 days after the application of differentiation medium (Fig. 9). Intriguingly, on the ABIKO iron plate, the amount of calcium deposits was greater. After 6-day culture in the differentiation medium, the expression levels of certain osteogenic marker genes, Runt-related transcription factor 2 Runx2, tissue-nonspecific alkaline phosphatese Alpl, Osteocalcin Bglap, and Osteopontin Spp1 were significantly upregulated in the cells on either ABIKO iron plates and control plastic dishes (Fig. 9). Moreover, Runx2, Bglap and Spp1 expression levels were much higher in the cells on ABIKO iron plates compared with those of the cells on culture dish (Fig. 9). In addition, without switching the differentiation medium, basal levels of Runx 2, Bglap, and Spp1 already increased in the cells (Fig. 9). These suggest that the possibility of further promoting differentiation into osteogenic cells.

## 4. Conclusions

Our results revealed the uniqueness of ABIKO iron, which allows not only mammalian cell attachment and proliferation but also greater biocompatibility for osteogenic and myotube differentiation without the need for a surface coating than that of conventional biomaterials. This should lead to the novel use of ABIKO iron as a therapeutic material in the continuously growing field of biomedical application. Therefore, we intend to investigate the long-term effects of ABIKO iron not only in vitro but also in vivo. In addition, production costs are still high, requiring more than $ 1,000,000 per kilogram. Currently, we are trying to reduce the cost to 1/10. Cost reduction through mass production and new refining technologies is a key issue for the future.

## Declaration of competing interest

The authors declare no competing interests.

## CRediT authorship contribution statement

**Luqman Khan:** Formal analysis, Data curation, Writing - original draft. **Katsumi Sato:** Conceptualization, Resources. **Shinichi Okuyama:** Conceptualization, Writing - review & editing. **Takeshi Kobayashi:** Formal analysis, Data curation, Resources, Writing - review & editing. **Kazumasa Ohashi:** Methodology, Resources. **Katsuya Hirasaka:** Formal analysis, Writing - original draft. **Takeshi Nikawa:**

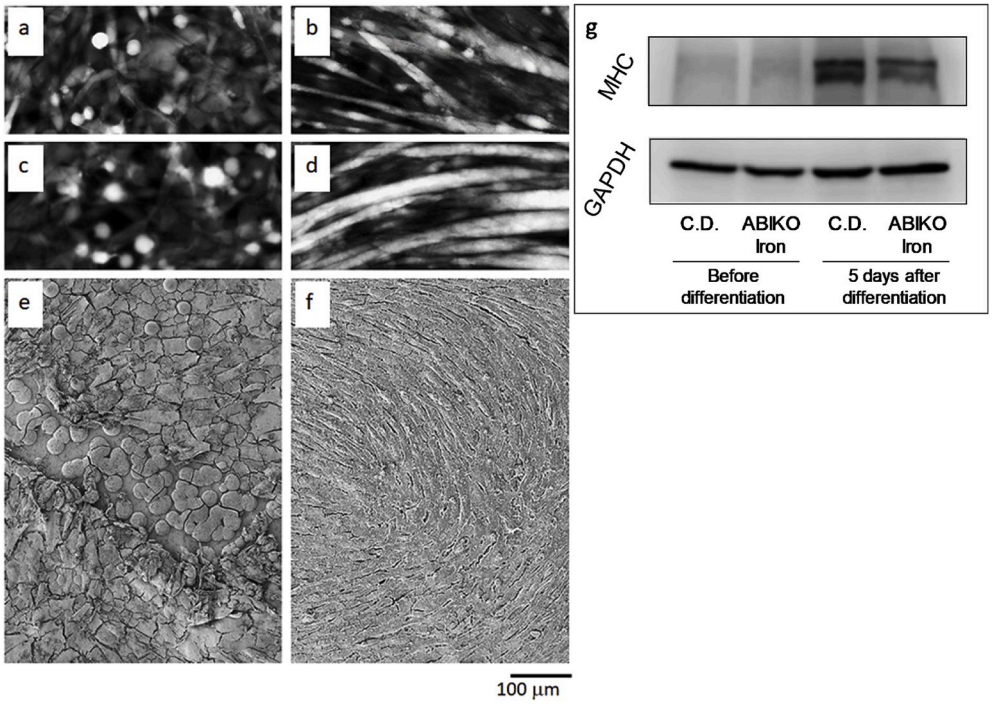


**Fig. 8.** C2C12 myoblast cells on ABIKO iron plate.

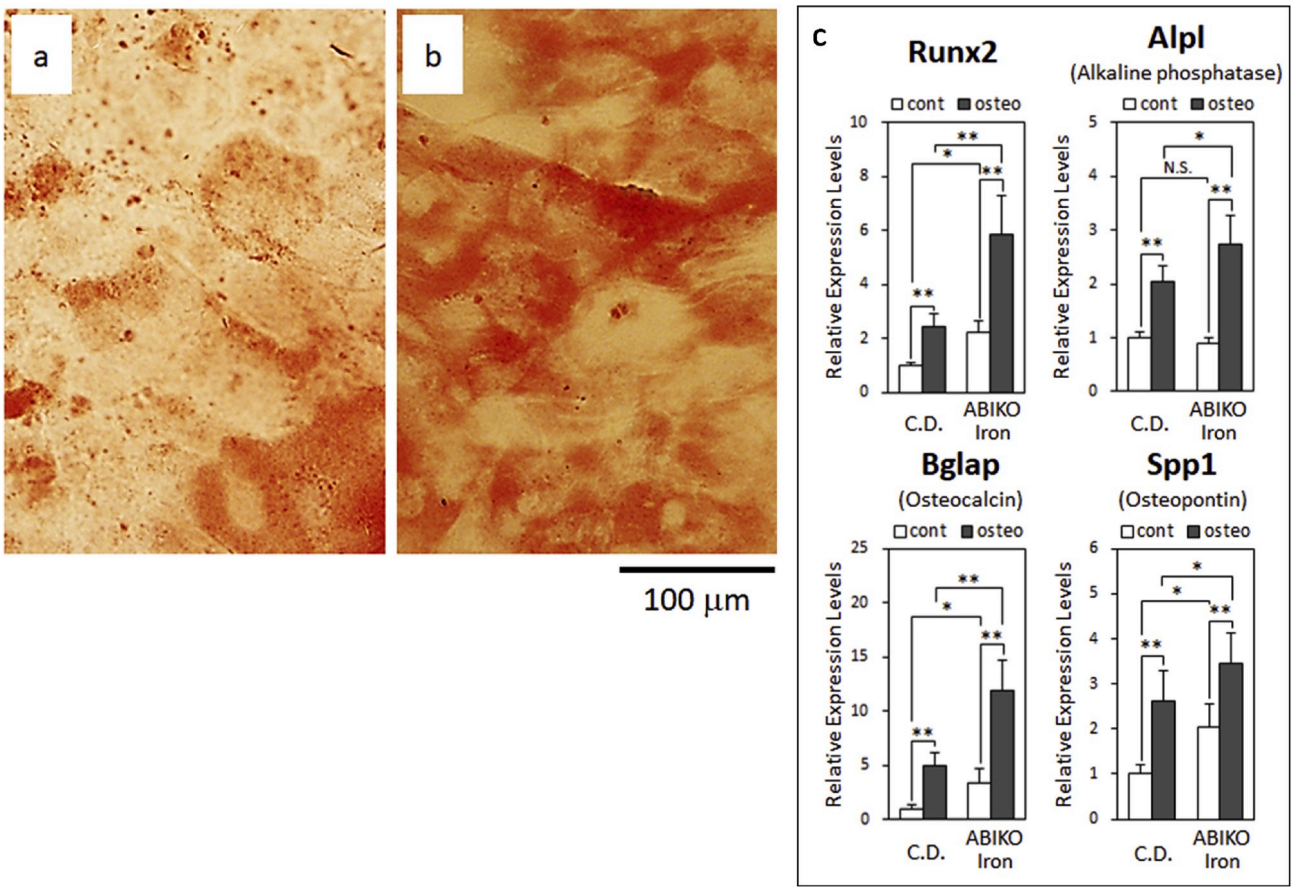


**Fig. 9.** Alizarin red S staining and osteogenic gene expression analyses of mesenchymal stem cells (MSCs).

Resources. **Kunio Takada:** Formal analysis. **Atsushi Higashitani:** Formal analysis, Funding acquisition, Writing - review & editing, Project administration. **Kenji Abiko:** Conceptualization, Resources, Project administration.

## Acknowledgements

We thank Dr. Mika Teranishi for critical reading of the manuscript. This work was funded in part by Advanced Research and Development Programs for Medical Innovation, Japan AMED-CREST (16814305). L.K. received a scholarship from the Ministry of Education, Culture, Sports, Science and Technology, Japan. This work based on a Patent PCT/JP 2018/189387 by K.A., A.H., S.O. and K.S.

## Appendix A. Supplementary data

Supplementary data to this article can be found online at https://doi.org/10.1016/j.jmbbm.2020.103744.

**(a)** ABIKO iron plate. **(b)** Abundant, normally shaped cells on the surface of the ABIKO iron plate. **(c)** Cells on the culture dish with the ABIKO iron plate. **(d)** Corrosion that appeared on the S45C steel plate. **(e)** No or little cells on the surface of the S45C steel plate. **(f)** Irregular cells on the surface of the culture dish with the S45C steel plate.

$FeSO_4$ was applied exogenously 12 h after inoculating $1 \times 10^5$ cells, and the cells were cultured for an additional 2 days before harvesting. **(a)** Control cells. **(b)** Cells to which $FeSO_4$ was applied at a final concentration of 0.01 mM in culture medium. **(c)** Cells with application of 1.0 mM $FeSO_4$. **(d)** Cells with application of 5.0 mM $FeSO_4$. **(e)** Confluence of MDCK–YFP-keratin-8 cells after 3 days of culture (means ± SD, n = 5). Data with the same letter did not differ significantly at the 5% level.

Alterations of relative expression levels of **(a)** heat shock protein HSP70 gene, **(b)** superoxide dismutase SOD1, **(c)** ataxia-telangiectasia mutated gene ATM, and **(d)** iron-responsive element-binding protein IRP2 were calculated with the expression level of GAPDH gene as the internal standard. Statistical significance was set at $^{**}p < 0.01$, using a Student's two-tailed t-test.

**(4a)** Cell confluence was measured on the culture dish (C.D.) and on each metal plate by fluorescence microscopy (means ± SD, n = 5). Data with the same letter did not differ significantly at the 5% level. **(4b)** Live images of YFP-keratin-8 fluorescent cells. **(i)** Control cells on C.D. (without metal plate). **(ii)** Cells on surface of ABIKO iron plate. **(iii)** Cells on surface of C.D. with ABIKO iron. **(iv)** Cells on surface of Cr–Co–Mo alloy plate. **(v)** Cells on surface of C.D. with Cr–Co–Mo alloy. **(vi)** Cells on surface of Ti–6Al–4V alloy plate. **(vii)** Cells on surface of C.D. with Ti–6Al–4V alloy.

**(a)** Thin coiled wire (0.5< mm diameter) made of ABIKO iron before use. **(b)** Cells on surface of ABIKO iron wire cultured for 3 days (yellow arrows). **(c)** Cells on surface of ABIKO iron wire cultured for additional 5 days. **(d)** Cells cultured for additional 5 days at the same magnification of panel b.

**(a)** Confluent cells on ABIKO iron plate. **(b)** Actively growing cells on ABIKO iron plate; the inoculum was diluted four-fold compared with that in panel A. **(c)** Higher magnification of panel B. On the surface of the ABIKO iron, thin film-like substances containing filopodia, which seems to be extracellular matrix released from cells, were observed (red dotted area indicated by a red arrow). **(d)** Poorly proliferating cells with expanded lamellipodia on the surface of a Cr–Co–Mo alloy plate. **(e)** Higher magnification of panel D. **(f)** Poorly growing cells with multiple blebs on a Ti–6Al–4V alloy plate. **(g)** Higher magnification of panel F. Scale bars represent 10 μm.

**(a)** After soaking 0.01 mg/ml FITC-labelled collagen solution, FITC

fluorescence on surface of slide glass, Ti–6Al–4V, and ABIKO iron plates were visualized with a fluorescent stereo microscopy. **(b)** FITC intensity was quantified by Image J software (±SD, $n = 5$). Data with the different letter significantly differed at the 5% level. Scale bar, 200 μm.

**(a)** Calcein AM stained C2C12 myoblast cells on a culture dish before differentiation for 3 days with the ABIKO iron. **(b)** Calcein AM stained C2C12 myoblast cells on a culture dish after differentiation for 5 days with the ABIKO iron. **(c)** C2C12 myoblast cells of the ABIKO iron plate before differentiation for 3 days. **(d)** C2C12 myoblast cells on the ABIKO iron plate after differentiation for 5 days. **(e)** Scanning electron microscope (SEM) image of cells in panel C. **(f)** SEM image of differentiated cells in panel d. **(g)** A differentiation marker for myotubes, Skeletal muscle myosin protein (MHC) levels were monitored in the C2C12 cells before and after differentiation by western blotting. GAPDH as control.

**(a)** MSCs on a culture dish after differentiation for 21 days in the presence of ABIKO iron. **(b)** Cells on the ABIKO iron plate after differentiation for 21 days. **(c)** Osteogenic marker genes, Runx2, Alpl, Bglap, and Spp1 expression levels were monitored in the cells after 6-day culture with (osteo) or without (cont) osteogenic differentiation induction by real-time RT PCR methods. *$p < 0.05$, **$p < 0.01$, and n. s. Not significant using a Student's two-tailed t-test.

## References


Abiko, K., Nakajima, T., Harima, N., Takaki, S., 1998. Preparation of 10 kg ingot of ultrapure iron. Phys. Status Solidi (a) 167, 347–355.

Abiko, K. Iron, 2002. Ultrahigh-purity. In: Buschow, K.H.J., Cahn, R.W., Flemings, M.C., Ilshner, B., Kramer, E.J., Mahajan, S., Veyssiere, P. (Eds.), Encyclopedia of Materials: Science and Technology, second ed. Elsevier Publishing, ISBN 978-0-08-043152-9. pp.1–9.

Bacakova, L., Filova, E., Parizek, M., Ruml, T., Svorcik, V., 2011. Modulation of cell adhesion, proliferation and differentiation on materials designed for body implants. Biotechnol. Adv. 29, 739–767.

BAM (Germany) COMAR Certificate for Primary Reference Material, ABIKO NanoMetal-A001 Ultrahigh Purity Iron (UHP Fe-01).

Bang, L.T., Filho, L.C., Engqvist, H., Xia, W., Persson, C., 2019. Synthesis and assessment of metallic ion migration through a novel calcium carbonate coating for biomedical implants. J. Biomed. Mater. Res. B Appl. Biomater. https://doi.org/10.1002/jbm.b.34399.

Besinis, A., Hadi, S.D., Le, H., Tredwin, C., Handy, R., 2017. Antibacterial activity and biofilm inhibition by surface modified titanium alloy medical implants following application of silver, titanium dioxide and hydroxyapatite nanocoatings. Nanotoxicology 11, 327–338.

Chou, D.-T., et al., 2013. In vitro and in vivo corrosion, cytocompatibility and mechanical properties of biodegradable Mg–Y–Ca–Zr alloys as implant materials. Acta Biomater. 9, 8518–8533.

Costa, B.C., et al., 2019. Vanadium ionic species from degradation of Ti-6Al-4V metallic implants: in vitro cytotoxicity and speciation evaluation. Mater. Sci. Eng. C 96, 730–739, 2019.

Fage, S.W., Muris, J., Jakobsen, S.S., Thyssen, J.P., 2016. Titanium: a review on exposure, release, penetration, allergy, epidemiology, and clinical reactivity. Contact Dermatitis 74, 323–345.

Fujiwara, S., Ohashi, K., Mashiko, T., Kondo, H., Mizuno, K., 2016. Interplay between Solo and keratin filaments is crucial for mechanical force–induced stress fiber reinforcement. Mol. Biol. Cell 27, 954–966.

Gomes, C.C., et al., 2011. Assessment of the genetic risks of a metallic alloy used in medical implants. Genet. Mol. Biol. 34, 116–121.

Halliwell, B., Gutteridge, J.M., 1990. Role of free radicals and catalytic metal ions in human disease: an overview. Methods Enzymol. 186, 1–85.

Hanawa, T., 2004. Metal ion release from metal implants. Mater. Sci. Eng. C 24, 745–752.

Lai, J.C., et al., 2008. Exposure to titanium dioxide and other metallic oxide nanoparticles induces cytotoxicity on human neural cells and fibroblasts. Int. J. Nanomed. 3, 533.

Li, H., Malyar, R.M., Zhai, N., Wang, H., Liu, K., Liu, D., Pan, C., Gan, F., Huang, K., Miao, J., Chen, X., 2019. Zinc supplementation alleviates OTA-induced oxidative stress and apotosis in MDCK cells by up-regulating metallothioneins. Life Sci. 234, 116735.

Marini, F., Luzi, E., Fabbri, S., Ciuffi, S., Sorace, S., Tognarini, I., Galli, G., Zonefrati, R., Sbaiz, F., Brandi, M.L., 2015. Osteogenic differentiation of adipose tissue-derived mesenchymal stem cells on nanostructured Ti6Al4V and Ti13Nb13Zr. Clin Cases Miner Bone Metab 12, 224–237.

Niinomi, M., 2002. Recent metallic materials for biomedical applications. Metall. Mater. Trans. 33, 477.

Oliveira, F., Rocha, S., Fernandes, R., 2014. Iron metabolism: from health to disease. J. Clin. Lab. Anal. 28 (3), 210–218.

Pacheco, K.A., 2019. Allergy to surgical implants. Clin. Rev. Allergy Immunol. 56, 72–85.

Puntarulo, S., 2005. Iron, oxidative stress and human health. Mol. Aspect. Med. 26, 299–312.

Santos-Coquillat, A., Mohedano, M., Martinez-Campos, E., Arrabal, R., Pardo, A., Matykina, E., 2019. Bioactive multi-elemental PEO-coatings on titanium for dental implant applications. Mater Sci Eng C Mater Biol Appl 97, 738–752.

Sidambe, A.T., 2014. Biocompatibility of advanced manufactured titanium implants—a review. Materials 7, 8168–8188.

Tibau, A.V., Grube, B.D., Velez, B.J., Vega, V.M., Mutter, J., 2019. Titanium exposure and human health. Oral Sci. Int. 16, 15–24. https://doi.org/10.1002/osi2.1001.

Vasconcelos, D.M., Santos, S.G., Lamghari, M., Barbosa, M.A., 2016. The two faces of metal ions: from implants rejection to tissue repair/regeneration. Biomaterials 84, 262–275.

Wang, Y., Yan, Y., Su, Y., Qiao, L., 2017. Release of metal ions from nano CoCrMo wear debris generated from tribo-corrosion processes in artificial hip implants. Mech Behav Biomed Mater 68, 124–133.

Wickman, G.R., Julian, L., Mardilovich, K., Schumacher, S., Munro, J., Rath, N., Zander, S.A., Mleczak, A., Sumpton, D., Morrice, N., Bienvenut, W.V., Olson, M.F., 2013. Blebs produced by actin-myosin contraction during apoptosis release damage-associated molecular pattern proteins before secondary necrosis occurs. Cell Death Differ. 20 (10), 1293–1305.

Yoshimura, T., Saitoh, K., Sun, L., Wang, Y., Taniyama, S., Yamaguchi, K., Uchida, T., Ohkubo, T., Higashitani, A., Nikawa, T., Tachibana, K., Hirasaka, K., 2018. Morin suppresses cachexia-induced muscle wasting by binding to ribosomal protein S10 in carcinoma cells. Biochem. Biophys. Res. Commun. 506, 773–779.